

# ChemComm

Chemical Communications

Accepted Manuscript

This article can be cited before page numbers have been issued, to do this please use: M. Li, Y. hu, H. Fu, X. Qu, Z. Xu and S. Zheng, *Chem. Commun.*, 2019, DOI: 10.1039/C9CC05274G.



This is an Accepted Manuscript, which has been through the Royal Society of Chemistry peer review process and has been accepted for publication.

Accepted Manuscripts are published online shortly after acceptance, before technical editing, formatting and proof reading. Using this free service, authors can make their results available to the community, in citable form, before we publish the edited article. We will replace this Accepted Manuscript with the edited and formatted Advance Article as soon as it is available.

You can find more information about Accepted Manuscripts in the [Information for Authors](#).

Please note that technical editing may introduce minor changes to the text and/or graphics, which may alter content. The journal's standard [Terms & Conditions](#) and the [Ethical guidelines](#) still apply. In no event shall the Royal Society of Chemistry be held responsible for any errors or omissions in this Accepted Manuscript or any consequences arising from the use of any information it contains.

## COMMUNICATION

**Pt embedded in carbon rods of N-doped CMK-3 as highly active and stable catalyst for catalytic hydrogenation reduction of bromate**

Minghui Li, Yuan Hu, Heyuan Fu, Xiaolei Qu, Zhaoyi Xu, Shourong Zheng\*

Received 00th January 20xx,  
Accepted 00th January 20xx

DOI: 10.1039/x0xx00000x

**Novel Pt-based catalyst with fine and homogeneous Pt particles embedded in carbon rods of N-doped CMK-3 was fabricated by a two-step infiltration method using SBA-15 as the template. Due to its fine particle size, N-containing functionality and effective embedment of Pt particles in carbon rods, the catalyst exhibited superior catalytic activity and stability in the liquid phase catalytic hydrogenation of bromate in water.**

Supported precious metal catalysts have been widely used in liquid phase catalytic hydrogenation under ambient conditions to remove pollutant, such as nitrate, perchlorate, bromate and chlorophenols.<sup>1-4</sup> However, leaching, aggregation or/and surface contamination of metal particles inevitably occur, leading to catalyst deactivation during the catalytic processes.<sup>5,6</sup> Numerous attempts have been made to avoid the deactivation of supported noble metal catalysts. For example, heteroatom doping (e.g., N-, S- or B-doping) was used to enhance metal-support interaction of noble metal catalysts supported on carbonaceous supports in order to alleviate catalyst deactivation.<sup>7,8</sup> Confining metal particles in the pores of zeolite, MOFs and mesoporous SiO<sub>2</sub> was confirmed to effectively suppress catalyst deactivation.<sup>9</sup> Very recently, embedment of metal particles beneath conductive carbon layers has been proved to be a prominent strategy to enhance catalyst stability. For example, Fu et al.<sup>10</sup> prepared a coated Ni/Al<sub>2</sub>O<sub>3</sub> catalyst with N-doped carbon layer, which exhibited a superior stability for catalytic hydrogenation reduction of 4-nitrochlorobenzene even under strong acidic conditions. In parallel, Li et al.<sup>11</sup> developed a stable and reusable coated carbon nanotube (CNT) supported Pd catalysts by a N-doped carbon shell and observed superior sintering resistance and high stability for catalytic Cr(VI) reduction. In contrast to their counterparts in the

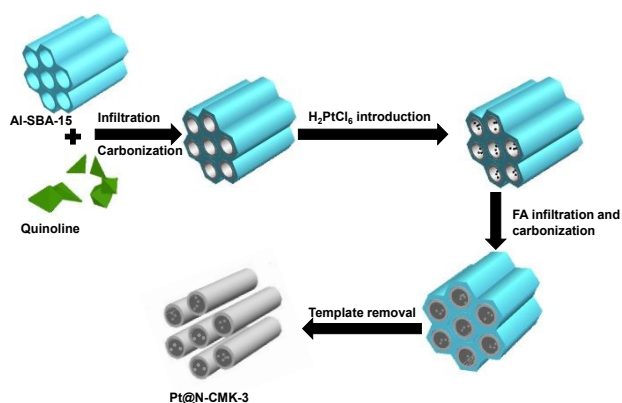
uncoated catalysts, metal particles of the coated catalyst were inaccessible for reactants, while the intimate contact between embedded metal particles and carbon overcoating resulted in unique metal-carbon heterojunctions, capable of evoking Mott-Schottky effect.<sup>12</sup> As a result, the carbon layers were activated and acted as catalytically active sites, on which H<sub>2</sub> could be adsorbed and activated.<sup>10,12</sup> Accordingly, enhanced stability of the coated catalysts was normally achieved at the cost of catalytic activities due to complete embedment of active metal particles beneath overcoatings despite of the formation of active metal-carbon heterojunctions.<sup>13,14</sup> Hence, fabrication of catalysts with both high stability and activity is still highly challenging.

Mesoporous carbon is generally considered as one of the best choices as catalyst supports due to its ordered pore structure, large surface area and accessible pore volume.<sup>15</sup> Herein, we report the fabrication of novel catalysts with highly dispersed Pt particles, which are embedded in the carbon rods of N-doped mesoporous carbon by a two-step infiltration method using SBA-15 as the template. In comparison with typical Pt catalyst coated by nonporous carbon layers (Pt/CNT@C), Pt catalysts embedded in the carbon rods of mesoporous carbon and N-doped mesoporous carbon (denoted as Pt@CMK-3 and Pt@N-CMK-3 respectively) had higher surface areas. Additionally, Pt@N-CMK-3 had a higher point of zero charge (PZC) than Pt@CMK-3 and Pt/CNT@C due to the presence of N-containing functionalities, which was likely beneficial for the adsorption of anionic pollutants on catalyst surface. The preparation procedure of the catalysts is illustrated in Scheme 1 and more synthesis details can be found in the experimental section of the electronic supplementary information (ESI†). In a typical procedure, a desired amount of quinoline was first infiltrated into a pre-synthesised aluminosilicate template (Al-SBA-15) to form hollow N-doped carbon tubes after catalytic polymerization of quinoline with the aid of acid sites of Al-SBA-15, followed by carbonization at 850 °C. Then, H<sub>2</sub>PtCl<sub>6</sub> was introduced into the hollow N-doped carbon tubes, followed by furfuryl alcohol infiltration and carbonization at 850 °C. Finally, the template Al-SBA-15 was removed using a HF solution to obtain the catalysts with Pt

State Key Laboratory of Pollution Control and Resource Reuse, Jiangsu Key Laboratory of Vehicle Emissions Control, School of the Environment, Nanjing University, Nanjing 210023, PR China

E-mail: [srzheng@nju.edu.cn](mailto:srzheng@nju.edu.cn); Tel: +86-25-89680373

† Electronic Supplementary Information (ESI) available: Materials synthesis, characterization methods, supplementary figures (Fig. S1 to S13), supplementary table (Table S1, S2) and calculations (Calculation S1 and S2). See DOI: 10.1039/x0xx00000x



**Scheme 1.** Schematic illustration of embedment of Pt in the carbon rods of N-doped CMK-3 using a two-step infiltration method.

particles embedded in the carbon rods of N-doped CMK-3. In comparison, Pt supported on N-doped CMK-3 (denoted as Pt/N-CMK-3) was also prepared by the conventional impregnation method.

The wide-angle and small-angle X-ray diffraction (XRD) patterns of the samples are presented in Fig. S1, ESI†. In the wide-angle XRD pattern of Pt(0.55)/N-CMK-3, two broad diffraction peaks at 24° and 43° were observed, corresponding to the (002) and (101) crystal planes of graphite structure from porous carbon material.<sup>16</sup> Additionally, strong diffraction peaks at 40° and 46° were assigned to the (110) and (200) planes of Pt particles with a face centered cubic (FCC) structure (ICDDPDF-2#00-004-0802). For Pt(0.39)@CMK-3 and Pt(0.42)@N-CMK-3, similar diffraction peaks corresponding to graphite structure of porous carbon material were observed. As for Pt(0.48)/CNT@C, strong diffraction peaks at 26°, 42° and 54° assigned to graphite structure of CNT support were observed (see Fig. S1(a), ESI†).<sup>18</sup> Notably, the absence of metallic Pt diffraction peaks in Pt(0.48)/CNT@C, Pt(0.39)@CMK-3 and Pt(0.42)@N-CMK-3 was likely due to complete embedment of Pt particles beneath carbon matrix and/or very high Pt dispersions (small Pt particle sizes). Small angle XRD patterns of SBA-15 template and the catalysts are shown in Fig. S1(b), ESI†. Well resolved (100), (110), and (200) peaks from highly ordered hexagonal mesoporous structure were observed on the catalysts, reflecting that the structure of SBA-15 template was perfectly duplicated in the catalysts.<sup>17</sup> N<sub>2</sub> adsorption-desorption isotherms are presented in Fig. S2, ESI† and the resulting parameters are listed in Table S1, ESI†. The samples gave type-IV isotherms with capillary condensation at relative pressures ( $p/p_0$ ) between 0.3 and 0.8, indicative of the existence of mesopores in the samples.<sup>19</sup> In comparison with Pt(0.48)/CNT@C, the catalysts with Pt particles embedded in the carbon rods of porous carbon had much higher surface areas and pore volumes. The surface composition of Pt(0.55)/N-CMK-3 and Pt(0.42)@N-CMK-3 was analyzed by X-ray photoelectron spectroscopy (XPS) and the results are compiled in Fig. S3, ESI†. In the two catalysts, similar N 1s peaks consisting of pyridinic, pyrrolic and graphitic N species were clearly observed. TEM images of the catalysts and the corresponding distribution histograms of the Pt particles are presented in Fig. S4, ESI†. The average Pt particle sizes of the catalysts were calculated based on a surface area weighted diameter

(calculation details presented in Calculation S1, ESI†) and the results are listed in Table S1, ESI†. For Pt(0.55)/N-CMK-3, uneven distribution and aggregation of Pt particles were clearly visible (see Fig. S4(a), ESI†). Similarly, Pt(0.48)/CNT@C presented a very broad distribution of Pt particles varying from 2 nm to 14 nm. Meanwhile, Pt/CNT wrapped by uniform carbon shells were clearly observed in Pt(0.48)/CNT@C and Pt particles located on the external surface of carbon shells were not identified, reflecting that Pt particles were completely embedded beneath carbon shells (see Fig. S4(b), ESI†). In contrast, fine and very even distributions of Pt particles were observed on Pt(0.39)@CMK-3 and Pt@N-CMK-3 (see Fig. S4(c)-(g), ESI†). The average Pt particle sizes of Pt(0.48)/CNT@C and Pt(0.55)/N-CMK-3 were calculated to be 7.54 nm and 6.46 nm, respectively, whereas given an similar Pt loading, the average Pt particle size of Pt(0.42)@N-CMK-3 was much smaller (2.38 nm). The fine Pt particles and very narrow Pt particle distributions of Pt@N-CMK-3 were likely due to the presence of N-containing functionalities, giving rise to enhanced metal-support interaction and Pt dispersion. Furthermore, confinement effects from hollow tubular structure effectively suppressed Pt particle aggregation during the carbonization process (see Scheme 1). As for the Pt@N-CMK-3 catalysts with varied Pt loading amounts (shown in Fig. S4(d)-(g), ESI†), the average Pt particle sizes of Pt(0.22)@N-CMK-3, Pt(0.42)@N-CMK-3, Pt(1.20)@N-CMK-3 and Pt(1.91)@N-CMK-3 were 1.92, 2.38, 4.56 and 5.84 nm, respectively, reflecting gradually grown Pt particle sizes with Pt loading amount. To further evaluate the exposed Pt particles, the chemisorption amount of CO was measured and the results were shown in Table S1, ESI†. The chemisorption amount of CO was 17.6 μmol g<sup>-1</sup> for Pt(0.55)/N-CMK-3 but below detection limit in all embedded and coated catalysts. Correspondingly, the energy-dispersive spectroscopy (EDS) mapping was conducted on Pt(0.55)/N-CMK-3 and Pt(0.42)@N-CMK-3 and the images are shown in Fig. S5, ESI†. Similar distributions of C and N elements were identified on the catalysts, whereas the much lower density of Pt element in Pt(0.42)@N-CMK-3 than that in Pt(0.55)/N-CMK-3 confirmed the effective embedment of Pt in carbon rods. The results clearly indicated that Pt particles of embedded and coated catalysts were inaccessible for reactants.

Bromate is a carcinogenic disinfection byproduct and reduction of bromate to bromide is an effective method to eliminate bromate pollution in water. The liquid phase catalytic hydrogenation reduction of bromate was used to evaluate the catalytic performances of the catalysts. The influence of catalyst support on catalytic bromate reduction was tested (results presented in Fig. S6, ESI†). The control experiment showed that bromate concentration was constant in the presence of support, while effective bromate reduction was observed in the presence of Pt containing catalysts, indicating that bromate was catalytically converted. Additionally, good mass balances were obtained on catalytic bromate reduction, reflecting that bromide was the sole product from bromate reduction. For catalytic bromate reduction, the initial activity calculated as the removal rate of bromate within initial 6 min was used in order to avoid the influence from intermediate and/or final products on kinetic evaluation. Bromate reduction on Pt(0.42)@N-CMK-3 with varied catalyst dosages was carried out to verify if the reactions were conducted in the absence of mass transfer limitation. The results showed that the initial activities normalized by catalyst dosage were nearly constant, indicative

of the absence of mass transfer limitation under our

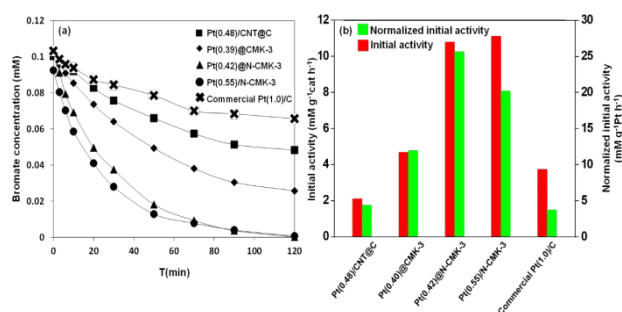


**Fig. 1.** (a) Catalytic hydrogenation reduction of bromate on different catalysts, (b) the initial activity and normalized initial activity with Pt loading amount. Reaction conditions: 0.1 mM bromate, 200 ml min<sup>-1</sup> H<sub>2</sub> flow and 0.1 g l<sup>-1</sup> catalyst at pH=5.6.

experimental conditions (see Fig. S7, ESI<sup>†</sup>).<sup>20</sup>

The catalytic reduction of bromate on the catalysts is presented in Fig. 1. The initial activities of Pt(0.48)/CNT@C, Pt(0.39)/CMK-3, Pt(0.42)/N-CMK-3, Pt(0.55)/N-CMK-3 and commercial Pt(1.0)/C for bromate reduction were 2.1, 4.7, 11.1, 10.8 and 3.7 mMgCat<sup>-1</sup>h<sup>-1</sup>, respectively, indicative of a decreasing order of Pt(0.55)/N-CMK-3 > Pt(0.42)/N-CMK-3 > Pt(0.39)/CMK-3 > commercial Pt(1.0)/C > Pt(0.48)/CNT@C. It was understandable that Pt(0.55)/N-CMK-3 exhibited the highest activity for bromate reduction due to the presence of exposed Pt active sites as indicated by CO chemisorption. However, effective bromate conversion was also identified on Pt(0.42)/N-CMK-3, Pt(0.39)/CMK-3 and Pt(0.48)/CNT@C although Pt particles of the catalysts were completely embedded beneath carbon overcoatings or in carbon rods. The results clearly confirmed that H<sub>2</sub> was capable of being activated and bromate could be reduced on the carbonaceous overcoatings of the catalysts with metal-carbon heterojunctions. Additionally, Pt(0.42)/N-CMK-3 displayed a slightly lower initial activity, but a higher Pt content normalized activity than Pt(0.55)/N-CMK-3 (see Fig. 1(b)). Notably, the initial activity of Pt(0.42)/N-CMK-3 was comparable or higher than those previously reported (see Table S2, ESI<sup>†</sup>). As carbonaceous surface acted as active sites, surface area was likely positively correlated to the catalytic activity of the catalyst. Notably, Pt(0.39)/CMK-3 has a specific surface area of 378.9 m<sup>2</sup> g<sup>-1</sup>, which was 22 times higher than that of Pt(0.48)/CNT@C, while the catalytic activity of Pt(0.39)/CMK-3 was only 2.2 times as much as that of Pt(0.48)/CNT@C, reflecting that the catalytic activities of the embedded catalysts were likely controlled by other factors instead of surface area of the catalyst (see more discussion below). As compared with Pt(0.39)/CMK-3, a higher activity was observed on Pt(0.42)/N-CMK-3, likely attributed to the presence of N-containing functionality with a higher PZC (6.57) (see Fig. S8, ESI<sup>†</sup>), resulting in the strong electrostatic attractive interaction between N-doped carbon surface and anionic bromate.<sup>21</sup> In parallel, the much higher activity of Pt(0.55)/N-CMK-3 was because of its higher Pt dispersion and enhanced bromate adsorption resulting from N-doping although commercial Pt(1.0)/C had a higher Pt loading.

To verify the role of bromate adsorption, the catalytic reduction of bromate with varied initial concentrations ( $C_0$ ) was carried out on Pt(0.42)/N-CMK-3, and the reaction data were fitted to the Langmuir–

Hinshelwood model (see Fig. S9, ESI<sup>†</sup>). The good linear relationship between  $1/r_0$  and  $1/C_0$  suggested

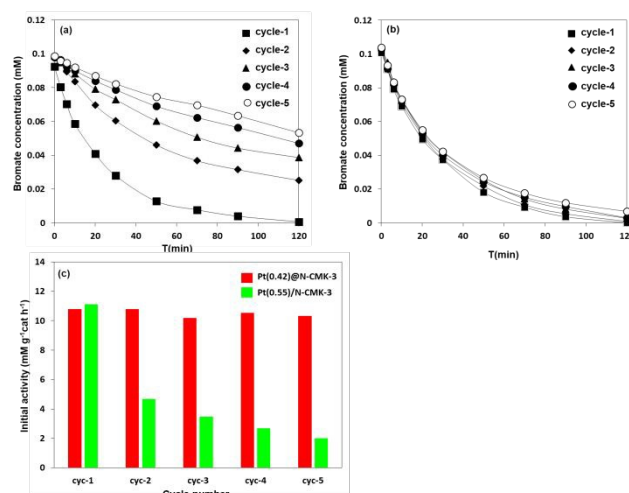


**Fig. 2.** The consecutive catalytic cycle of (a) Pt(0.55)/N-CMK-3, (b) Pt(0.42)/N-CMK-3, and (c) the corresponding initial activities of catalysts in each reaction cycle. Reaction conditions: 0.1 mM bromate, 200 ml min<sup>-1</sup> H<sub>2</sub> flow and 0.1 g l<sup>-1</sup> catalyst at pH=5.6.

that bromate reduction could be well described by Langmuir–Hinshelwood model and the catalytic conversion of bromate was controlled by the adsorption of bromate. Additionally, increasing pH of bromate reduction on Pt(0.42)/N-CMK-3 led to a monotonical decrease of initial bromate conversion, indicative of a strong pH dependency (see Fig. S10, ESI<sup>†</sup>). Such a strong pH dependence was ascribed to the electrostatic interaction between bromate and the catalysts. At low pH, anionic bromate was electrostatically adsorbed on positively charged catalyst surface, while increasing pH led to substantially suppressed adsorption of anionic bromate because catalyst surface was negatively charged at high pH, giving rise to suppressed bromate conversion.

It was notable that the catalysts with embedded metal-carbon heterojunctions is prone to evoking Mott-Schottky effect, resulting in electron transfer between Fermi levels of metal and CN rod.<sup>22</sup> Accordingly, electron transfer efficiency was strongly dependent on interfaces between metal particles and CN rods. To evaluate the interface effects, Pt@N-CMK-3 catalysts with varied Pt loadings and Pt particle sizes were prepared and the catalytic bromate reduction on the catalysts is presented in Fig. S11(a), ESI<sup>†</sup>. The initial activity increased from 6.7 to 18.0 mMgCat<sup>-1</sup>h<sup>-1</sup> with the increase of Pt loading from 0.22 to 1.91 wt.%, reflecting a more effective bromate removal with the increase of Pt-CN interface. The initial activities of the catalysts were normalized by interface areas of Pt-CN heterojunctions assuming spherical Pt particles and close contact between Pt particles and CN rods in the catalysts and the results are presented in Fig. S11(b), ESI<sup>†</sup>. Despite of varied Pt particle sizes, specific surface areas and Pt loading amounts, the catalysts exhibited nearly constant interface area normalized reaction rates for bromate reduction, clearly indicative of the crucial role of interface between metallic Pt and CN rods.

To test catalyst stability, the consecutive catalytic reduction of bromate was conducted on Pt(0.55)/N-CMK-2 and Pt(0.42)/N-CMK-3 and the results are presented in Fig. 2. After five consecutive catalytic cycles, the initial activity of

Pt(0.55)/N-CMK-3 rapidly decreased from 11.1 to 2.0 mMgCat<sup>-1</sup>h<sup>-1</sup>. In parallel, ICP analysis indicated that the Pt content of Pt(0.55)/N-CMK-3 decreased by 58.2% after five catalyst recycles. Additionally, TEM results indicated that Pt particle size of the used catalyst was smaller than that of fresh one (See Fig. S12 (a) and (b), ESI<sup>†</sup>). Hence, the obvious deactivation of Pt(0.55)/N-CMK-3 was mainly ascribed to the loss of large Pt particles during the catalytic reaction due to weak interactions between Pt particles and carbon support despite of the presence of N-containing functionalities. In contrast, the initial activity of used Pt@N-CMK-3 after five catalyst cycles was 10.3 mMgCat<sup>-1</sup>h<sup>-1</sup>, which was nearly identical to that of fresh catalyst (10.8 mMgCat<sup>-1</sup>h<sup>-1</sup>), indicative of negligible catalyst deactivation and very high catalytic stability. Furthermore, Pt contents of the used and fresh Pt(0.42)@N-CMK-3 were measured to be 0.42 and 0.41 wt.%, respectively. In parallel, Pt particle size of used Pt(0.42)@N-CMK-3 (2.46 nm) was identical to that of fresh one (2.38 nm) (Results shown in Fig. S12 (c) and (d), ESI<sup>†</sup>). The results clearly showed that the novel structure of Pt@N-CMK-3 with embedded Pt particles in carbon rods could effectively suppress catalyst deactivation. Accordingly, the high catalytic stability was also observed on Pt(1.91)@N-CMK-3 (Results shown in Fig. S13, ESI<sup>†</sup>).

In summary, we have fabricated a novel Pt@N-CMK-3 catalyst with fine Pt particles embedded in N-doping carbon rods using a two-step infiltration method. The fine Pt particles as well as even Pt particle distribution are obtained as a result of the confinement effect from the ordered mesoporous structure of CMK-3. N-doping and high surface area of carbon matrix provide more appropriate active sites for the adsorption and reduction of bromate. Furthermore, the embedment of Pt particles in carbon rods of N-doping CMK-3 matrix effectively increases the interface areas between Pt and carbon rods and meanwhile inhibits leaching and aggregation of Pt particles. Accordingly, Pt@N-CMK-3 displays superior catalytic performances in the liquid catalytic hydrogenation of bromate to Pt/N-CMK-3, Pt@CMK-3 and Pt/CNT@C. The findings in this work demonstrate that embedding metal particles in porous carbon matrix provides a new avenue to effectively utilize noble metals in heterogeneous catalysis.

This work was supported by the National Natural Science Foundation of China (No. 21577056) and Outstanding Youth Foundation of Jiangsu Province of China (No. BK20190301).

## Conflicts of interest

There are no conflicts to declare.

## Notes and references

- (a) R. A. W. Johnstone and A. H. Wilby, *Chem. Rev.*, 1985, **85**, 129; (b) S. Horold, K.-D. Vorlop, T. Tacke and M. Sell, *Catal. Today*, 1993, **17**, 21.
- (a) K. D. Hurley and J. R. Shapley, *Environ. Sci. Technol.*, 2007, **41**, 2044; (b) H. Chen, Z. Y. Xu, H. Q. Wan, J. Z. Zheng, D. Q. Yin and S. R. Zheng, *Appl. Catal. B-Environ.*, 2010, **96**, 307.
- H. Chen, Y. Shao, Z. Y. Xu, H. Q. Wan, Y. Q. Wan, S. R. Zheng and D. Q. Zhu, *Appl. Catal. B-Environ.*, 2011, **105**, 255.
- F. B. Su, Z. Q. Tian, C. K. Poh, Z. Wang, S. H. Lim, Z. L. Liu and J. Y. Lin, *Chem. Mater.*, 2010, **22**, 832.

- G. W. Zhan and H. C. Zeng, *Chem. Mater.*, 2015, **27**, 776.
- M. S. Ide, D. D. Falcone and R. J. Davis, *J. Catal.*, 2014, **311**, 295.
- M. Terrones, A. Jorio, M. Endo, A. M. Rao, Y. A. Kim, T. Hayashi, H. Terrones, J. C. Charlier, G. Dresselhaus and M. S. Dresselhaus, *Mater. Today*, 2004, **7**, 30.
- (a) X. Kong, C. Chen and Q. Chen, *Chem. Soc. Rev.*, 2014, **43**, 2841; (b) Q. Zhang, W. Huang, J. M. Hong and B. Y. Chen, *Chem. Eng. J.*, 2018, **343**, 662.
- (a) V. Bernales, D. Yang, J. Yu, G. Gümüşlü, C. Cramer, B. Gates and L. Gagliardi, *ACS Appl. Mater. Interfaces*, 2017, **9**, 33511; (b) P. Serna and B. C. Gates, *Acc. Chem. Res.*, 2014, **47**, 2612; (c) M. Yang, J. L. Liu, S. Lee, B. Zugic, J. Huang and L. F. Allard, *J. Am. Chem. Soc.*, 2015, **137**, 3470; (d) J. Canivet, S. Aguado, Y. Schuurman and D. Farrusseng, *J. Am. Chem. Soc.*, 2013, **135**, 4195; (e) M. Yang, S. Li, Y. Wang, J. A. Herron, Y. Xu, L. F. Allard, S. Lee, J. Huang and M. Mavrikakis, *Science*, 2014, **346**, 1498.
- T. Fu, M. Wang, W. M. Cai, Y. M. Cui, F. Gao, L. M. Peng, W. Chen and W. P. Ding, *ACS Catal.*, 2014, **4**, 2536.
- M. H. Li, J. He, Y. Q. Tang, J. Y. Sun, H. Y. Fu, Y. Q. Wan, X. L. Qu, Z. Y. Xu and S. R. Zheng, *Chemosphere*, 2019, **217**, 742.
- (a) T. Chen, S. Q. Guo, J. Yang, Y. D. Xu, J. Sun, D. L. Wei, Z. X. Chen, B. Zhao and W. P. Ding, *ChemPhysChem*, 2017, **18**, 3454; (b) K. X. Zhang, H. Su, H. H. Wang, J. J. Zhang, S. Y. Zhao, W. W. Lei, X. Wei, X. H. Li and J. S. Chen, *Adv. Sci.*, 2018, **5**, 1800062.
- H. N. Pham, A. E. Anderson, R. L. Johnson, T. J. Schwartz, B. J. O'Neill, P. Duan, K. Schmidt-Rohr, J. A. Dumesic and A. K. Datye, *ACS Catal.*, 2015, **5**, 4546.
- B. Sun, T. J. Fu, and H. C. Zeng, *Chem. Commun.*, 2018, **54**, 7030.
- (a) F. Jiao and H. Frei, *Chem. Commun.*, 2010, **46**, 2920; (b) F. Jiao and H. Frei, *Angew. Chem. Int. Ed.*, 2009, **48**, 1841.
- (a) X. Ji, P. S. Herle, Y. Rho and L. F. Nazar, *Chem. Mater.*, 2007, **19**, 374; (b) Z. Wen, X. Wang, S. Mao, Z. Bo, H. Kim, S. Cui, G. Lu, X. Feng and J. Chen, *Adv. Mater.*, 2012, **24**, 5610.
- (a) J. Xiao, X. Pan, S. Guo, P. Ren and X. Bao, *J. Am. Chem. Soc.*, 2014, **137**, 477; (b) S. Yang, X. Zhang, H. Mi, and X. Ye, *J. Power Sources*, 2008, **175**, 26.
- (a) X. K. Li, W. J. Ji, J. Zhao, S. J. Wang and C. T. Au, *J. Catal.*, 2005, **236**, 181; (b) L. Borchardt, E. Kockrick, P. Wollmann, S. Kaskel, M. M. Guron, L. G. Sneddon and D. Geiger, *Chem. Mater.*, 2010, **22**, 4660.
- (a) D. Zhao, J. Feng, Q. Huo, N. Melosh, G. H. Fredrickson, B. F. Chmelka and G. D. Stucky, *Science*, 1998, **279**, 548; (b) S. Jun, S. H. Joo, R. Ryoo, M. Kruk, M. Jaroniec, Z. Liu, T. Ohsuna and O. Terasaki, *J. Am. Chem. Soc.*, 2000, **122**, 10712.
- (a) G. Yuan and M. A. Keane, *Chem. Eng. Sci.*, 2003, **58**, 257; (b) O. M. Ilinitch, F. P. Cuperus, L. V. Nosova and E. N. Gribov, *Catal. Today*, 2000, **56**, 137.
- (a) G. P. Mane, S. N. Talapaneni, C. Anand, S. Varghese, H. Lwai, Q. M. Ji, K. Ariga and T. Mori, A. Vinu, *Adv. Funct. Mater.*, 2012, **22**, 3596; (b) P. Zhang, F. Jiang and H. Chen, *Chem. Eng. J.*, 2013, **234**, 195.
- (a) X. H. Li and M. Antonietti, *Chem. Soc. Rev.*, 2013, **42**, 6593; (b) Y. Zhou, K. Neyerlin, T. S. Olson, S. Pylypenko, J. Bult, H. N. Dinh, T. Gennett, Z. Shao and R. O'Hayre, *Energy Environ. Sci.*, 2010, **3**, 1437.